Supplement of Atmos. Chem. Phys., 17, 6611–6629, 2017
https://doi.org/10.5194/acp-17-6611-2017-supplement

Atmospheric Chemistry and Physics
Open Access
EGU

Supplement of

Influence of urban pollution on the production of organic particulate matter from isoprene epoxydiols in central Amazonia

Suzane S. de Sá et al.

Correspondence to: Scot T. Martin (scot_martin@harvard.edu)

S1. Instrumentation

S1.1 Aerosol Mass Spectrometry: set up and operation

Online measurements of organic and sulfate mass concentrations measured in this study were made by a High-Resolution Time-of-Flight Aerosol Mass Spectrometer (AMS, Aerodyne Research Inc.) (DeCarlo et al., 2006; Canagaratna et al., 2007). The AMS provided real-time measurements of bulk non-refractory particle chemical composition (organic, sulfate, nitrate, ammonium, chloride) and chemically resolved mass-diameter distribution. Air was sampled through a critical orifice and enters an aerodynamic lens, which focused the submicron particles into a narrow beam (Zhang et al., 2004). Particles traveled through a sizing chamber to reach a porous tungsten inverted-cone vaporizer at 600 °C, and non-refractory components volatilized. The gaseous molecules were then ionized through electron impact (70 eV), and the ions were measured by time-of-flight mass spectrometry. The high mass resolution allowed for the distinction of ions having the same nominal mass but different elemental composition. Data analysis was performed using standard AMS software (*SQUIRREL* 1.56D, *PIKA* 1.14G) (webpage: http://cires1.colorado.edu/jimenez-group/ToFAMSResources/ToFSoftware/index.html).

Aerosol particles were sampled through a cyclone (URG-2000-30EH) which had a size cut of 2.5 um for a flow of 16.7 L min^{-1}. The sampled flow (14.9 to 16.3 L min^{-1}) traveled through a stainless steel tube for about 1.5 m. The flow was then split in two: a 4-m line for sampling (1.2 or 2.6 L min^{-1}) and a line (13.7 L min^{-1}) for exhaust. The sampling flow changed between 1.2 and 2.6 L min^{-1} according to the flow set up of the Scanning Mobility Particle Sizer (SMPS), which was sampling in parallel to the AMS. The sampling flow then entered a poly-tube Nafion dryer (Perma Pure, model PD-100T). Drying prior to entering the instrument

container aimed at avoiding water condensation in the line inside the container, which was always kept at lower temperatures than outside (i.e., trailer temperature was around 23 °C during daytime). RH measured after the poly-tube dryer and inside the container was at 40 to 80%. Within the container, a subflow (0.6 or 3 L min^{-1}) was passed through a mono-tube Nafion dryer (Perma Pure, model MD-110) to reach RH < 40%. A flow of 0.09 L min^{-1} was sampled by the AMS, and the remaining flow of 0.5 or 2.9 L min^{-1} was sampled by the SMPS. The ambient air sampling line was integrated to a valve switching system, which alternated the AMS/SMPS sampling between the unprocessed ambient air and air processed by oxidation flow reactors or a thermal denuder. The unprocessed ambient air (used for this analysis) was sampled for 4 out of 8 min, constituting half of the total acquired data set.

Due to expected low mass concentrations and to secondary need for the low-sensitivity high-resolution data, the AMS was operated for most of the time in medium-resolution V-mode ($\Delta m/m$ = 2200 at *m/z* 44), which was used for mass quantification. High-resolution W-mode ($\Delta m/m$ = 4000 at *m/z* 44) was acquired for one of every six days. These data were used to aid choice of ions to fit. When only V-mode data were acquired, the instrument was operated in "mass spectrum" sub-mode for 180 s and in "particle-time-of-flight" sub-mode for 60 s. When W-mode data were also collected, the "W-mass-spectrum" sub-mode was operated for 60 s, the "V-mass-spectrum" sub-mode ran for 120 s, and "V-particle-time-of-flight" sub-mode ran for 60 s. Both ways of operation corresponded to 4 min for each cycle, allowing for synchronization to the valve switching system.

The AMS sensitivity and the ammonium relative ionization efficiency (RIE) were calibrated every five days using dried ammonium nitrate particles having a mobility diameter of 400 nm. An interpolated curve of the obtained values, corresponding to RIE = 4.3 ± 0.2, was

used for mass calculation corrections. The sulfate RIE was calibrated using ammonium sulfate a few times during the campaign, and the average value of 0.9 ± 0.1 was applied to the entire campaign. The collection efficiency (CE) was determined as 1.0 for IOP1 according to volume comparison to the two co-located Scanning Mobility Particle Sizers (Figure S6). Volume of black carbon (BC) accounted for 8 ± 6 % of the total volume measured by SMPS, for an assumed density of 1.8 g cm^{-3} for BC. Since BC data were limited, the abscissa of Figure S6 was not subtracted by BC contribution. This CE value was consistent with that used for the AMAZE-08 in the wet season of 2008 (Chen et al., 2009).

S1.2 Semi-Volatile Thermal desorption Aerosol Gas Chromatography: set up and operation

Online measurements of organic tracer compounds in the particle and gas phases were made by a Semi-Volatile Thermal desorption Aerosol Gas chromatograph (SV-TAG). This instrument is described in detail elsewhere (Isaacman et al., 2014). Its operation is briefly presented here.

Air was sampled at 20 L min^{-1} from the center stream of a flow of 200 L min^{-1} through a 15.24 cm (OD) stainless steel duct at a height of approximately 5 m above ground level. The flow was then divided into two channels, passing through a PM1 cyclone at 10 L min^{-1}, each containing a custom Filter Collection and Thermal Desorption cell (F-CTD). The F-CTD quantitatively collected and retained both particle- and gas-phase compounds. A multi-channel carbon denuder (MAST Carbon) was used to remove all gases upstream of one collection cell. In this way, two samples were simultaneously collected: a “particle” sample and a “total” gas-plus-particle sample. Samples were thermally desorbed from the cells subjected to a ramping temperature from 30 to 310 °C (35 °C min^{-1}) into a helium stream that was 80% saturated with

MSTFA (N-Methyl-N-(trimethylsilyl) trifluoroacetamide). Hydroxyl groups were converted into silyl esters and ethers. Analytes were transferred to the GC column, and the sample was analyzed through a commercially available GC/MS (7890A/5975C; Agilent Technologies). The chromatographic data were analyzed using the publicly available software *TAG ExploreR and iNtegration* (Isaacman-VanWertz and Sueper).

Compounds were quantified using isotopically labeled internal standards to correct for run-to-run variability in sample transfer efficiency and instrument response. Regular multi-point calibrations were made of approximately 100 authentic standards. Pentaerythritol-2-^{13}C was used for 2-methyltetrols and C_5-alkene triols. The uncertainty in mass concentration was approximately 15% (Isaacman et al., 2014). C_5-alkene triols were quantified using the calibration factor of 2-methyltetrols under the assumption of an identical total ion response. An absence of an authentic standard results in unconstrained uncertainty in mass concentration of 30 of 50% (Jaoui et al., 2005).

S1.3 NO_y measurements

The NO_y measured included the following species: NO, NO_2, HNO_3, particle nitrate, RNO_3, and PAN. Measurements were made by a custom analyzer designed by Air Quality Design (AQD; http://www.airqualitydesign.com). The analyzer was based on two commercial oxides of nitrogen detectors made by Thermo Scientific (Model 42i TLE) and extensively modified by AQD. An external, temperature-controlled inlet box was mounted at 10 m above ground level.

The instrument contained both a research grade LED photolysis cell for converting NO_2 into NO and a heated molybdenum converter for converting total NO_y into NO. One channel, leading from the photolysis cell to one 42i TLE detector, alternated every minute between NO

and NO_x by switching the LED photoloysis cell on/off. The other channel, leading from the molybdenum converter to the second 42i TLE detector, measured total NO_y. The detectors internally measured zero based on pre-reaction of the sample with ozone. Instrument response was measured by addition of NO in zero air at the sampling point (10 m). Converter efficiency was measured by gas-phase titration of the NO standard to NO_2. An HNO_3 source was sampled every other day. The calibration unit was a Thermo Scientific Model 146i calibrator equipped with gas-phase titration and a permeation oven. The raw NO_y measurements, reported at a resolution of 10 s, were averaged into bins of 30 min to filter for local events not representative of the larger scale chemical processes that form the scope of this study.

S2. Positive Matrix Factorization and the IEPOX-SOA factor

The time series of mass spectra of organic material measured by the AMS was analyzed by positive matrix factorization (PMF) using a standard analysis toolkit (Ulbrich et al., 2009). High-resolution, V-mode data were used. The PMF solution was based on minimization of the "Q-value" or "PMF quality-of fit parameter", meaning the sum of the weighed squared residuals for a chosen number of factors. The interpretation of the physical significance of the AMS PMF factors took into account correlations with quantities simultaneously measured by other instruments. The solution consisted of six factors, and the present study focuses on one of the derived factors, labeled "IEPOX-SOA". de Sá (in preparation) focuses on presentation of the other factors.

The profile of the resolved IEPOX-SOA factor is shown in Figure S1. A key characteristic is intensity at $C_5H_6O^+$ (*m/z* 82) (Hu et al., 2015). In addition, a prominent signal at $C_4H_5^+$ (*m/z* 53) is observed, which has also been reported as characteristic of the IEPOX-SOA factor (Hu et al., 2015). The IEPOX-SOA factor is also relatively highly oxidized, as expressed

by f_{44} = 0.15 and oxygen to carbon atomic ratio O:C = 0.80, applying the calibration described in Canagaratna et al. (2015).

Technical diagnostics of the six-factor solution are presented in Figure S2 and more extensively described in (de Sá, in preparation). Panel b shows the quality of fit parameter $Q/Q_{expected}$ (Ulbrich et al., 2009) as a function of the number of factors, suggesting that the solution should have at least three factors. Panel a shows a great reduction in the structure of the total residuals when going from the five-factor to the six-factor solution. The six-factor solution also offered more meaningful factor profiles ("mass spectra") (de Sá, in preparation). Panel c shows $Q/Q_{expected}$ as a function of the rotational ambiguity parameter f_{peak} (Ulbrich et al., 2009) for the six-factor solution. A plausible range for f_{peak} was determined according to the best practice of limiting $Q/Q_{expected}$ to a value that does not exceed 0.1% of the minimum value (occurring at $f_{peak} = 0$). The default value of $f_{peak} = 0$ was chosen for the final six-factor solution, since no significant improvements in the external validation of the factors were observed. Moreover, the IEPOX-SOA factor resolved in the six-factor solution had a very robust time trend across a range of rotations in the solution (Figure S2d). As f_{peak} varied, the correlation of factor loading with C5-alkene triols concentrations remained approximately constant, even as some features of the factor profile changed significantly, such as the relative signals of $C_5H_6O^+$ and CO_2^+, respectively $f(C_5H_6O)$ and $f(CO_2)$, as well as the magnitude of factor loadings and consequently the ratio f.

The loading of the IEPOX-SOA factor may be an overestimate or an underestimate of the atmospheric concentration of the IEPOX-derived PM (brown dashed lines in Figure 1). In respect to overestimate, the AMS mass spectrum observed in laboratory studies for the uptake of IEPOX by acidic sulfate particles is statistically equal to that obtained for the uptake of isoprene

139 photo-oxidation products, yet IEPOX accounted for only half of those products (Liu et al., 2015).
140 The implication is that the uptake of non-IEPOX species can lead to a similar AMS spectrum.
141 Pathways of PM production from condensation of multifunctional hydroperoxides lead to a
142 distinct mass spectrum from IEPOX pathways, and are not expected to be highly active under the
143 acidic particle conditions of these experiments (Riva et al., 2016), leaving a large mass fraction
144 of produced PM unexplained. The combination of AMS vaporization at 600 °C and ionization by
145 electron impact at 70 eV may convert IEPOX-derived and non-IEPOX-derived molecules into
146 similar groups of ions, which then give rise to a similar mass spectrum. The SV-TAG, which
147 uses desorption temperatures up to 310 °C and thus can also induce thermal decomposition of
148 some molecules, might also result in an in-common analyte (i.e., tracer) between IEPOX-derived
149 and non-IEPOX-derived molecules, thereby precluding a constraint on any possible overestimate
150 by the AMS factor (Isaacman-VanWertz et al., 2016; Lopez-Hilfiker et al., 2016). For these
151 reasons, the loading of the IEPOX-SOA factor might overestimate IEPOX-derived PM
152 concentrations by accounting for other isoprene oxidation products that are not produced through
153 the IEPOX intermediate.

154 In respect to underestimate, the loading of the IEPOX-SOA factor may not capture the
155 entire particle-phase carbon footprint that originated from IEPOX uptake. Extensive atmospheric
156 processing, such as reactions with hydroxyl radicals or photolysis, can partly eliminate the initial
157 products of IEPOX uptake (Kroll et al., 2009; Bateman et al., 2011; Epstein et al., 2014; Hu et
158 al., 2015; Hu et al., 2016). The IEPOX-originated carbon can still be inside the particle, yet it no
159 longer contributes to the loading of the IEPOX-SOA factor because of an altered mass spectrum
160 for some molecules. Atmospheric reactions gradually homogenize particle composition and
161 properties, and the AMS spectra can become more uniform (Jimenez et al., 2009). Specifically,

the ratio of signal intensity at *m*/*z* 44 to that at *m*/*z* 43 increases, and the relative intensity of *m*/*z* 82 decreases (Ng et al., 2011; Hu et al., 2015). This modified organic material, which originally entered the particle phase through IEPOX uptake, may then contribute to the loading of PMF factors other than IEPOX-SOA, such as the oxidized organic factors broadly labeled as "OOA" (Zhang et al., 2005). For these several reasons, the IEPOX-SOA factor loading might be an underestimate of IEPOX-derived PM concentrations.

S3. Comparison of background and polluted cases

The presence of a pollution plume at T3 is indicated by a combination of several external measured variables, including particle number, ozone, and NO_y concentrations. The definition of background and polluted cases aimed at selecting afternoons that were associated with extreme values of those variables. Conditions entailing concentration of ozone at around 10 ppb or less, particle number concentration of less than 500 cm^{-3}, and NO_y concentrations of less than 1 ppb were collectively a strong indicative of a background case. Conditions including ozone concentrations upward of 30 ppb, particle number concentration above 2000 cm^{-3}, and NO_y concentrations around 1.5 ppb or above indicated pollution. Measurements of these variables onboard the G-1 aircraft confirmed what the ground measurements suggested on the several days that the G-1 flew overhead.

Examples of these supporting data are illustrated in Figure 3 for the chosen background and polluted days (March 3 and 13, 2014, respectively) composing the primary case study analyzed in the main text. A few other afternoons, representative of these two extremes of background and polluted cases, were selected from the campaign time series and are depicted in Figure S4. The top panel shows cases of background conditions, and the bottom panel shows cases of polluted conditions. The local wind direction observed for the polluted cases generally

characterized by easterlies, as consistent with Manaus direction, whereas for the background cases it tends to diverge from that prevailing direction. The cases within each category are ordered from left to right in ascending order of IEPOX-SOA factor loadings.

Sulfate concentrations had a wide range of values, even for background conditions (Figure S4), as discussed in the main text. Meteorological conditions such as overcast (lower photoxidation activity) and rain events (higher wet deposition), as seen on March 20 and March 23, are some of the factors that control particle number and mass concentration (sulfate and organic compounds). These factors help to explain the natural variability in sulfate mass concentration. By comparison, on a sunny day, with winds mostly coming from the northeast direction, as exemplified by February 16 and March 3, sulfate mass concentrations can be around 0.3 μg m^{-3} or more, values which are also typical of some polluted days (bottom panel). Both the factor loading and the ratio f increased with increasing sulfate (rows 2 and 3 of top panel), when NO_y levels were approximately the same. A comparison of February 16 and March 3 shows in addition the importance of NO_y concentration: for similar concentrations of sulfate and organic PM and similar meteorological conditions, the case having lower NO_y concentrations (0.4 to 0.5 ppb on March 3 as compared to 0.7 to 0.8 ppb on February 16) was associated with considerably higher absolute and relative factor loadings.

For the polluted cases shown in Figure S4, NO_y concentrations were variable between and within cases, ranging from 1 ppb up to 7 ppb. Larger sulfate mass concentrations (from left to right) were associated with larger absolute and relative factor loadings, analogous to what was observed for background cases. A comparison between March 3 and 13 (i.e., background and polluted; Figure 4) shows that for similar sulfate concentrations but higher NO_y levels March 13 had considerably lower factor loadings. The case of February 9 (polluted) illustrates that the

factor loadings did not exceed 0.4 μg m^{-3} and *f* did not exceed 0.2 even at rarely high sulfate concentrations in the wet season, reaching 0.9 μg m^{-3}. This finding is attributed to the high NO concentrations, as implied by NO_y concentrations of 3 ppb and greater, that suppressed IEPOX production.

These cases illustrate the possible wide range of observed sulfate mass concentrations under background conditions, in great part overlapping with typical values of polluted conditions. The cases also demonstrate that the trend in observed IEPOX-SOA factor loadings and ratio *f*, both within each category (background or polluted conditions) and between them, can be consistently explained by the roles that sulfate and NO exert on the production of IEPOX-derived PM.

S4. Sulfate and particle acidity estimates in the context of field studies

The underlying relative importance of direct compared to indirect roles of sulfate on the formation of IEPOX-derived PM is not well understood. Sulfate can play a direct role as a nucleophile in the reaction of formation of organosulfates from IEPOX (Surratt et al., 2007b; Nguyen et al., 2014). Organosulfates, however, are believed to constitute only a fraction of the IEPOX-derived PM (Hu et al., 2015). Particle acidity, an indirect effect of sulfate, has been shown to drive IEPOX-derived PM production in several lab studies (Surratt et al., 2007a; Kuwata et al., 2015; Lewandowski et al., 2015). Nevertheless, the acidity effect observed in laboratories is not as clearly observed in field studies, wherein pH estimates have typically been employed as a proxy for acidity (Budisulistiorini et al., 2013; Lin et al., 2013; Worton et al., 2013; Budisulistiorini et al., 2015; Xu et al., 2015). The present study corroborates those findings and further argues that this apparent conflict can be reasoned by taking into account that both the estimate and the end-use of pH may be problematic in the context of field studies.

231 Firstly, a reliable estimate of pH is often hard to obtain. In the case of the present study,
232 some difficulties were imposed by data availability. Gas-phase measurements of NH_3 or HNO_3
233 were not available for performing "forward" mode calculations in thermodynamic models or gas-
234 particle phase partitioning calculations, which have been suggested as the best method to predict
235 pH (Hennigan et al., 2015). Co-located independent measurements of ion concentrations (e.g., by
236 chromatograph) were not available to confirm the ion balance obtained by AMS measurements
237 (Figure S7).
238 Bearing these caveats in mind, the analysis presented in the main text using sulfate as a
239 predictor for IEPOX-SOA was replicated here using pH in place of sulfate. Figure S8 is
240 analogous to Figure 6a. pH was estimated for IOP1 using AMS measurements of mass
241 concentrations of inorganic ions (sulfate, ammonium, nitrate, and chloride) and measurements of
242 RH and temperature. The E-AIM model II (Clegg et al., 1998) was employed. The final pH was
243 calculated taking into account both the inorganic water predicted by the model and the organic
244 water estimated from organic hygroscopicity κ_{org} values (Thalman, in preparation), in a similar
245 fashion as described by Guo et al. (2015). Figure S8 shows that pH, as calculated herein and for
246 the caveats herein, does not work well as a predictor for IEPOX-SOA factor loading. Figure S9
247 is analogous to Figure 7. Figure S9 shows that, although the overall dependencies on NO_y are
248 similar to analysis of the data by sulfate, the separation by pH yields groups that have less
249 distinct trends and ranges among them.
250 In addition to difficulties associated with generating accurate estimates of pH, there is an
251 inconsistency between the timescales of estimated particle acidity and IEPOX-SOA factor
252 loadings that may preclude underlying correlations to emerge. The estimated pH makes use of
253 instantaneous RH and temperature values and is therefore an instantaneous estimate of pH. They

can change in timescales of 15 min or less giving mixing in the boundary layer, for example. On the other hand, sulfate mass concentrations and IEPOX-SOA factor loadings are variables representative of processes of longer time scales of hours and days. By not containing any information on the particle acidity history in the past hours or days, the calculated instantaneous pH may fail in capturing the true effect of acidity on the chemical formation of IEPOX-derived PM. The RH cycling history of sulfate particles has been demonstrated to mediate the extent of IEPOX-derived PM production (Wong et al., 2015). Moreover, sulfate, by being intrinsically related to particle acidity and at the same time a species of congruent lifetime with secondary organic material, may in fact be a better proxy to capture the history of particle acidity than estimates of pH. For these different reasons, sulfate rather than pH is used in the analysis herein. The understanding, however, is that sulfate represents effects beyond those of the direct chemical role of sulfate. In analogy to pH, this discussion also extends to the use of sulfate rather than instantaneous particle water content as the predictor of IEPOX-SOA factor loadings.

S5. Five subsets of data based on NO_y concentrations

The data subsets and fits shown in Figure 6 are shown in separate panels in Figure S5. Once a trend of decreasing fit slope with increasing NO_y concentration was identified, the number of data subsets was defined as the minimum necessary to have subsets of at least 100 data points (of a total of 888) to allow for robust statistics and that were also cohesive (as measured by R^2) and non-redundant (i.e., of different fit lines).

The coloring by date in Figure S5 shows that there is no apparent correlation between levels of NO_y concentration or goodness of fit with different time periods within IOP1. Meteorological variables such as solar radiation, temperature, and RH (not shown) are also not able to delineate any clear pattern in the data, either within or among groups.

Although a linear bivariate statistical analysis for the IEPOX-SOA factor in sulfate and NO_y concentrations at first appears attractive, the underlying chemical processes were not linear, as reflected in the relationship between IEPOX-derived PM and NO_y concentrations. Moreover, sulfate and NO_y concentrations were not independent variables. For these reasons, a linear bivariate analysis is not appropriate, and a subset analysis was pursued instead.

S6. Details and assumptions of the model

The solution to the differential Equation 1 is as follows:

$$M(t) = \frac{\alpha_P k_P}{\alpha_L k_L} + e^{\alpha_L k_L t}\left(M_0 - \frac{\alpha_P k_P}{\alpha_L k_L}\right) \quad \text{(S1)}$$

for which the subscript 0 indicates initial (background) conditions, i.e., immediately before the airmass passes over Manaus. For the transport from Manaus to T3, $t = \tau_{tr}$, and the variable M represents the IEPOX-derived PM mass concentrations at T3.

The zero-order production rate coefficient k_P and the first-order loss rate coefficient k_L are lumped parameters representative of several production and loss processes, respectively. A first assumption is that they are constant over the course of four hours. In hand with that assumption, a constant boundary layer height throughout the integration time is assumed. The τ values represent the time required under afternoon conditions to significantly affect the IEPOX-derived PM mass concentration by the corresponding processes. For afternoon time periods, observations show that $dM/dt > 0$ over tropical forests in the absence of pollution (Chen et al., 2009; Chen et al., 2015).The parameter τ_P, corresponding to a first order process, therefore represents an instantaneous quantity in the transient system. For simplicity of presentation, τ_P is defined in reference to M_0, although defining it in relation to M_{bg} or M_{pol} does not alter the main conclusions presented herein.

In terms of loss processes, represented by the rate coefficient k_L, IEPOX-derived PM may be lost by three main mechanisms: heterogeneous oxidation against OH, condensed-phase reactions, and dry deposition. The lifetime of IEPOX-derived PM against heterogeneous oxidation is estimated at around two weeks for an OH concentration of 10^6 molecules cm^{-3} (Hu et al., 2016). Lifetime of IEPOX products against particle-phase reactions has not yet been reported but is expected to be at least several days. A value of one week is used here. The lifetime of PM against deposition is on the order of a week. The overall loss process is then approximated in the model as the sum of these three processes, which leads to an estimate of overall loss rate coefficient $k_L = 0.015\ h^{-1}$ (overall characteristic time of 2.8 days).

In respect to wet deposition along the track from Manaus to the T3 site, strong convection imports background regional air, and for this reason strong wet deposition is mathematically equivalent in the model developed herein to a trajectory that does not pass over Manaus, i.e., background conditions. Weak wet deposition represents a mixing of polluted and background air masses, giving rise to intermediate NO_y concentrations. Entrainment on the plume edges as well as with the free troposphere is mathematically similar to wet deposition in the model framework. Thus entrainment and wet deposition, without directly contributing to k_L, are indirectly incorporated in the developed model based on their effects on NO_y concentration.

In terms of production processes, represented by the rate coefficient k_P, IEPOX-derived PM is produced by multigenerational chemistry of isoprene photooxidation and reactive uptake. Model Case 1 investigated the sensitivity of pollution enhancement ratio and absolute mass concentration of IEPOX-derived PM to its production rate coefficient. After constrained by observations, the estimated interval for k_P was [0.07, 0.13] $\mu g\ m^{-3}\ h^{-1}$. In addition, values of $k_P >$ 0.2 $\mu g\ m^{-3}\ h^{-1}$ are unlikely given the rare observation (<1%) of $M_{bg} > 1 \mu g\ m^{-3}$.

The obtained range can be compared to estimates of total production rate of organic material from diameter growth rates. Firstly, a relative production rate of 1:3 for IEPOX-derived PM to total organic PM is assumed based on the following. IEPOX-derived PM is estimated to contribute 34% on average to total organic PM in central Amazonia under background conditions (Chen et al., 2015). For assumptions of equal first order loss rate coefficients for all organic material, a mass concentration ratio of 1:3 for IEPOX-derived PM to total organic material implies a ratio of 1:3 in their production rate coefficients k_P. As a consequence, the estimated range for total organic material is [0.21, 0.39] μg m^{-3} h^{-1}. For the estimate of organic material production based on growth rates, an average growth rate of 10 nm h^{-1} (Kulmala et al., 2004) is assumed. Further assumptions are a range of particle number concentration of 500 to 1000 cm^{-3} and of initial diameter of 20 to 100 nm, typical of background conditions in the Amazon. The obtained range of organic material production from growth rate estimates is therefore 0.02 to 0.32 μg m^{-3} h^{-1}, which is comparable to the range constrained by the model.

In terms of the influence of Manaus plume on the production and loss processes, the following assumptions were made. The acceleration of the oxidant cycle in the plume implies that $\alpha_L > 1$. Under plume conditions, OH concentrations observed at the T3 site increased by a factor of three compared to background conditions (Martin et al., 2017; Kim, in preparation). A proportional increase in the loss rate of IEPOX-derived PM by OH heterogeneous chemistry in the plume is expected. While the OH loss mechanism (of characteristic time of two weeks) is accelerated by three fold in the plume, dry deposition and condensed phase reactions (both of assumed characteristic times of a week) are held constant. As a result, the overall loss rate is enhanced by two fold, i.e., $\alpha_L = 2$ is assumed.

Concerning the production enhancement factor, the interception of ISOPOO radicals by NO in the pollution plume as well as the faster consumption of intermediate gas-phase species by the enhanced OH and O_3 concentrations implies $\alpha_P < 1$. The assumption is that the production of IEPOX almost halts in the plume, and $\alpha_P = 0.1$. This assumption is supported by measured gas-phase concentrations of ISOPOOH at the T3 site, which dropped by 90% when NO_y concentrations increased from 0.5 ppb to 2 ppb (Liu et al., 2016). This observation and the associated model assumption are a reflection of the lifetimes of the chemical species discussed: in contrast to the abovementioned lifetimes on order of a week for organic particle material against loss processes, the lifetimes of the gaseous species are significantly shorter. Isoprene and ISOPOOH have a lifetime on the order of a few hours (Eddingsaas et al., 2010; St. Clair et al., 2015), and IEPOX has a lifetime of a few hours to a day for an OH concentration of 10^6 molecules cm^{-3} (Jacobs et al., 2013; Bates et al., 2014).

Supplementary References

Bateman, A. P., Nizkorodov, S. A., Laskin, J., and Laskin, A.: Photolytic processing of secondary organic aerosols dissolved in cloud droplets, Phys. Chem. Chem. Phys., 13, 12199-12212, 2011, 10.1039/C1CP20526A.

Bates, K. H., Crounse, J. D., St. Clair, J. M., Bennett, N. B., Nguyen, T. B., Seinfeld, J. H., Stoltz, B. M., and Wennberg, P. O.: Gas phase production and loss of isoprene epoxydiols, J. Phys. Chem. A, 118, 1237-1246, 2014, 10.1021/jp4107958.

Budisulistiorini, S. H., Canagaratna, M. R., Croteau, P. L., Marth, W. J., Baumann, K., Edgerton, E. S., Shaw, S. L., Knipping, E. M., Worsnop, D. R., Jayne, J. T., Gold, A., and Surratt, J. D.: Real-time continuous characterization of secondary organic aerosol derived from isoprene epoxydiols in downtown Atlanta, Georgia, using the Aerodyne Aerosol Chemical Speciation Monitor, Environ. Sci. Technol., 47, 5686-5694, 2013, 10.1021/es400023n.

Budisulistiorini, S. H., Li, X., Bairai, S. T., Renfro, J., Liu, Y., Liu, Y. J., McKinney, K. A., Martin, S. T., McNeill, V. F., Pye, H. O. T., Nenes, A., Neff, M. E., Stone, E. A., Mueller, S., Knote, C., Shaw, S. L., Zhang, Z., Gold, A., and Surratt, J. D.: Examining the effects of anthropogenic emissions on isoprene-derived secondary organic aerosol formation during the 2013 Southern Oxidant and Aerosol Study (SOAS) at the Look Rock, Tennessee ground site, Atmos. Chem. Phys., 15, 8871-8888, 2015, 10.5194/acp-15-8871-2015.

Canagaratna, M. R., Jayne, J. T., Jimenez, J. L., Allan, J. D., Alfarra, M. R., Zhang, Q., Onasch, T. B., Drewnick, F., Coe, H., Middlebrook, A., Delia, A., Williams, L. R., Trimborn, A. M., Northway, M. J., DeCarlo, P. F., Kolb, C. E., Davidovits, P., and Worsnop, D. R.: Chemical and microphysical characterization of ambient aerosols with the aerodyne

aerosol mass spectrometer, Mass Spectrom. Rev., 26, 185-222, 2007, 10.1002/mas.20115.

Canagaratna, M. R., Jimenez, J. L., Kroll, J. H., Chen, Q., Kessler, S. H., Massoli, P., Hildebrandt Ruiz, L., Fortner, E., Williams, L. R., Wilson, K. R., Surratt, J. D., Donahue, N. M., Jayne, J. T., and Worsnop, D. R.: Elemental ratio measurements of organic compounds using aerosol mass spectrometry: characterization, improved calibration, and implications, Atmos. Chem. Phys., 15, 253-272, 2015, 10.5194/acp-15-253-2015.

Chen, Q., Farmer, D. K., Schneider, J., Zorn, S. R., Heald, C. L., Karl, T. G., Guenther, A., Allan, J. D., Robinson, N., Coe, H., Kimmel, J. R., Pauliquevis, T., Borrmann, S., Pöschl, U., Andreae, M. O., Artaxo, P., Jimenez, J. L., and Martin, S. T.: Mass spectral characterization of submicron biogenic organic particles in the Amazon Basin, Geophys. Res. Lett., 36, L20806, 2009, 10.1029/2009GL039880.

Chen, Q., Farmer, D. K., Rizzo, L. V., Pauliquevis, T., Kuwata, M., Karl, T. G., Guenther, A., Allan, J. D., Coe, H., Andreae, M. O., Pöschl, U., Jimenez, J. L., Artaxo, P., and Martin, S. T.: Submicron particle mass concentrations and sources in the Amazonian wet season (AMAZE-08), Atmos. Chem. Phys., 15, 3687-3701, 2015, 10.5194/acp-15-3687-2015.

Clegg, S. L., Brimblecombe, P., and Wexler, A. S.: Thermodynamic model of the system H^+-NH_4^+-SO_4^{2-}-NO_3^--H_2O at tropospheric temperatures, J. Phys. Chem. A, 102, 2137-2154, 1998, 10.1021/jp973042r.

de Sá, S. S.: Anthropogenic emissions affect the sources and composition of submicron particulate matter in central Amazonia in the wet season, in preparation.

DeCarlo, P. F., Kimmel, J. R., Trimborn, A., Northway, M. J., Jayne, J. T., Aiken, A. C., Gonin, M., Fuhrer, K., Horvath, T., Docherty, K. S., Worsnop, D. R., and Jimenez, J. L.: Field-

deployable, high-resolution, time-of-flight aerosol mass spectrometer, Anal. Chem., 78, 8281-8289, 2006, 10.1021/ac061249n.

Eddingsaas, N. C., VanderVelde, D. G., and Wennberg, P. O.: Kinetics and products of the acid-catalyzed ring-opening of atmospherically relevant butyl epoxy alcohols, J. Phys. Chem. A, 114, 8106-8113, 2010, 10.1021/jp103907c.

Epstein, S. A., Blair, S. L., and Nizkorodov, S. A.: Direct photolysis of α-pinene ozonolysis secondary organic aerosol: effect on particle mass and peroxide content, Environ. Sci. Technol., 48, 11251-11258, 2014, 10.1021/es502350u.

Guo, H., Xu, L., Bougiatioti, A., Cerully, K. M., Capps, S. L., Hite Jr, J. R., Carlton, A. G., Lee, S. H., Bergin, M. H., Ng, N. L., Nenes, A., and Weber, R. J.: Fine-particle water and pH in the southeastern United States, Atmos. Chem. Phys, 15, 5211-5228, 2015, 10.5194/acp-15-5211-2015

Hu, W. W., Campuzano-Jost, P., Palm, B. B., Day, D. A., Ortega, A. M., Hayes, P. L., Krechmer, J. E., Chen, Q., Kuwata, M., Liu, Y. J., de Sá, S. S., McKinney, K., Martin, S. T., Hu, M., Budisulistiorini, S. H., Riva, M., Surratt, J. D., St. Clair, J. M., Isaacman-Van Wertz, G., Yee, L. D., Goldstein, A. H., Carbone, S., Brito, J., Artaxo, P., de Gouw, J. A., Koss, A., Wisthaler, A., Mikoviny, T., Karl, T., Kaser, L., Jud, W., Hansel, A., Docherty, K. S., Alexander, M. L., Robinson, N. H., Coe, H., Allan, J. D., Canagaratna, M. R., Paulot, F., and Jimenez, J. L.: Characterization of a real-time tracer for isoprene epoxydiols-derived secondary organic aerosol (IEPOX-SOA) from aerosol mass spectrometer measurements, Atmos. Chem. Phys., 15, 11807-11833, 2015, 10.5194/acp-15-11807-2015.

Hu, W. W., Palm, B., Day, D., Campuzano-Jost, P., Krechmer, J., Peng, Z., De Sá, S. S., Martin, S. T., Alexander, M. L., Baumann, K., Hacker, L., Kiendler-Scharr, A., Koss, A., De Gouw, J., Goldstein, A. H., Seco, R., Sjostedt, S., Park, J.-H., Guenther, A., Kim, S., Canonaco, F., Prevot, A., Brune, W., and Jimenez, J. L.: Long lifetime of ambient isoprene epoxydiols-derived Secondary Organic Aerosol (IEPOX-SOA) against OH oxidation and evaporation, Atmos. Chem. Phys. Disc., 2016, doi: 10.5194/acp-2016-418.

Isaacman-VanWertz, G. and Sueper, D.: TERN: TAG ExploreR and iNtegration https://sites.google.com/site/terninigor/.

Isaacman-VanWertz, G., Yee, L. D., Kreisberg, N. M., Wernis, R., Moss, J. A., Hering, S. V., de Sá, S. S., Martin, S. T., Alexander, M. L., Palm, B. B., Hu, W., Campuzano-Jost, P., Day, D. A., Jimenez, J. L., Riva, M., Surratt, J. D., Viegas, J., Manzi, A., Edgerton, E., Baumann, K., Souza, R., Artaxo, P., and Goldstein, A. H.: Ambient Gas-Particle Partitioning of Tracers for Biogenic Oxidation, Env. Sci. Technol., 2016, 10.1021/acs.est.6b01674.

Isaacman, G., Kreisberg, N., Yee, L., Worton, D., Chan, A., Moss, J., Hering, S., and Goldstein, A.: Online derivatization for hourly measurements of gas-and particle-phase semi-volatile oxygenated organic compounds by thermal desorption aerosol gas chromatography (SV-TAG), Atmos. Meas. Tech., 7, 4417-4429, 2014, 10.5194/amt-7-4417-2014.

Jacobs, M. I., Darer, A. I., and Elrod, M. J.: Rate constants and products of the OH reaction with isoprene-derived epoxides, Environ. Sci. Technol., 47, 12868-12876, 2013, 10.1021/es403340g.

Jaoui, M., Kleindienst, T., Lewandowski, M., Offenberg, J., and Edney, E.: Identification and quantification of aerosol polar oxygenated compounds bearing carboxylic or hydroxyl

groups. 2. Organic tracer compounds from monoterpenes, Environ. Sci. Technol., 39, 5661-5673, 2005, 10.1021/es048111b.

Jimenez, J. L., Canagaratna, M. R., Donahue, N. M., Prevot, A. S. H., Zhang, Q., Kroll, J. H., DeCarlo, P. F., Allan, J. D., Coe, H., Ng, N. L., Aiken, A. C., Docherty, K. S., Ulbrich, I. M., Grieshop, A. P., Robinson, A. L., Duplissy, J., Smith, J. D., Wilson, K. R., Lanz, V. A., Hueglin, C., Sun, Y. L., Tian, J., Laaksonen, A., Raatikainen, T., Rautiainen, J., Vaattovaara, P., Ehn, M., Kulmala, M., Tomlinson, J. M., Collins, D. R., Cubison, M. J., Dunlea, J., Huffman, J. A., Onasch, T. B., Alfarra, M. R., Williams, P. I., Bower, K., Kondo, Y., Schneider, J., Drewnick, F., Borrmann, S., Weimer, S., Demerjian, K., Salcedo, D., Cottrell, L., Griffin, R., Takami, A., Miyoshi, T., Hatakeyama, S., Shimono, A., Sun, J. Y., Zhang, Y. M., Dzepina, K., Kimmel, J. R., Sueper, D., Jayne, J. T., Herndon, S. C., Trimborn, A. M., Williams, L. R., Wood, E. C., Middlebrook, A. M., Kolb, C. E., Baltensperger, U., and Worsnop, D. R.: Evolution of organic aerosols in the atmosphere, Science, 326, 1525-1529, 2009, 10.1126/science.1180353.

Kim, S., in preparation.

Kroll, J. H., Smith, J. D., Che, D. L., Kessler, S. H., Worsnop, D. R., and Wilson, K. R.: Measurement of fragmentation and functionalization pathways in the heterogeneous oxidation of oxidized organic aerosol, Phys. Chem. Chem. Phys., 11, 8005-8014, 2009, 10.1039/B905289E.

Kulmala, M., Vehkamäki, H., Petäjä, T., Dal Maso, M., Lauri, A., Kerminen, V. M., Birmili, W., and McMurry, P. H.: Formation and growth rates of ultrafine atmospheric particles: a review of observations, J. Aerosol Sci., 35, 143-176, 2004, http://dx.doi.org/10.1016/j.jaerosci.2003.10.003.

Kuwata, M., Zorn, S. R., and Martin, S. T.: Using elemental ratios to predict the density of organic material composed of carbon, hydrogen, and oxygen, Environ. Sci. Technol., 46, 787-794, 2011, 10.1021/es202525q.

Kuwata, M., Liu, Y., McKinney, K., and Martin, S. T.: Physical state and acidity of inorganic sulfate can regulate the production of secondary organic material from isoprene photooxidation products, Phys. Chem. Chem. Phys., 17, 5670-5678, 2015, 10.1039/C4CP04942J.

Lewandowski, M., Jaoui, M., Offenberg, J., Krug, J., and Kleindienst, T.: Atmospheric oxidation of isoprene and 1, 3-butadiene: influence of aerosol acidity and relative humidity on secondary organic aerosol, Atmos. Chem. Phys., 15, 3773-3783, 2015, 10.5194/acp-15-3773-2015.

Lin, Y.-H., Knipping, E., Edgerton, E., Shaw, S., and Surratt, J. D.: Investigating the influences of SO_2 and NH_3 levels on isoprene-derived secondary organic aerosol formation using conditional sampling approaches, Atmos. Chem. Phys., 13, 8457-8470, 2013, 10.5194/acp-13-8457-2013.

Liu, Y., Kuwata, M., Strick, B. F., Geiger, F. M., Thomson, R. J., McKinney, K. A., and Martin, S. T.: Uptake of epoxydiol isomers accounts for half of the particle-phase material produced from isoprene photooxidation via the HO_2 pathway, Environ. Sci. Technol., 49, 250-258, 2015, 10.1021/es5034298.

Liu, Y., Brito, J., Dorris, M. R., Rivera-Rios, J. C., Seco, R., Bates, K. H., Artaxo, P., Duvoisin, S., Keutsch, F. N., Kim, S., Goldstein, A. H., Guenther, A. B., Manzi, A. O., Souza, R. A. F., Springston, S. R., Watson, T. B., McKinney, K. A., and Martin, S. T.: Isoprene

photochemistry over the Amazon rain forest, Proc. Natl. Acad. Sci. USA, 113, 6125-6130, 2016, 10.1073/pnas.1524136113.

Lopez-Hilfiker, F. D., Mohr, C., D'Ambro, E. L., Lutz, A., Riedel, T. P., Gaston, C. J., Iyer, S., Zhang, Z., Gold, A., Surratt, J. D., Lee, B. H., Kurten, T., Hu, W. W., Jimenez, J., Hallquist, M., and Thornton, J. A.: Molecular composition and volatility of organic aerosol in the Southeastern US: implications for IEPOX derived SOA, Environ. Sci. Technol., 2200–2209, 2016, 10.1021/acs.est.5b04769.

Martin, S. T., Artaxo, P., Machado, L. A. T., Manzi, A. O., Souza, R. A. F., Schumacher, C., Wang, J., Andreae, M. O., Barbosa, H. M. J., Fan, J., Fisch, G., Goldstein, A. H., Guenther, A., Jimenez, J. L., Pöschl, U., Silva Dias, M. A., Smith, J. N., and Wendisch, M.: Introduction: observations and modeling of the green ocean Amazon (GoAmazon2014/5), Atmos. Chem. Phys., 16, 4785-4797, 2016, 10.5194/acp-16-4785-2016.

Martin, S. T., Artaxo, P., Machado, L., Manzi, A. O., Souza, R. A. F., Schumacher, C., Wang, J., Biscaro, T., Brito, J., Calheiros, A., Jardine, K., Medeiros, A., Portela, B., Sá, S. S. d., Adachi, K., Aiken, A. C., Albrecht, R., Alexander, L., Andreae, M. O., Barbosa, H. M. J., Buseck, P., Chand, D., Comstock, J. M., Day, D. A., Dubey, M., Fan, J., Fast, J., Fisch, G., Fortner, E., Giangrande, S., Gilles, M., Goldstein, A. H., Guenther, A., Hubbe, J., Jensen, M., Jimenez, J. L., Keutsch, F. N., Kim, S., Kuang, C., Laskin, A., McKinney, K., Mei, F., Miller, M., Nascimento, R., Pauliquevis, T., Pekour, M., Peres, J., Petäjä, T., Pöhlker, C., Pöschl, U., Rizzo, L., Schmid, B., Shilling, J. E., Dias, M. A. S., Smith, J. N., Tomlinson, J. M., Tóta, J., and Wendisch, M.: The Green ocean Amazon Experiment

(GoAmazon2014/5) observes pollution affecting gases, aerosols, clouds, and rainfall over the rain forest, B. Am. Meteorol. Soc., 2017, doi:10.1175/BAMS-D-15-00221.1.

Ng, N., Canagaratna, M., Jimenez, J., Chhabra, P., Seinfeld, J., and Worsnop, D.: Changes in organic aerosol composition with aging inferred from aerosol mass spectra, Atmos. Chem. Phys., 11, 6465-6474, 2011, 10.5194/acp-11-6465-2011.

Nguyen, T. B., Coggon, M. M., Bates, K. H., Zhang, X., Schwantes, R. H., Schilling, K. A., Loza, C. L., Flagan, R. C., Wennberg, P. O., and Seinfeld, J. H.: Organic aerosol formation from the reactive uptake of isoprene epoxydiols (IEPOX) onto non-acidified inorganic seeds, Atmos. Chem. Phys., 14, 3497-3510, 2014, 10.5194/acp-14-3497-2014.

Riva, M., Budisulistiorini, S. H., Chen, Y., Zhang, Z., D'Ambro, E. L., Zhang, X., Gold, A., Turpin, B. J., Thornton, J. A., Canagaratna, M. R., and Surratt, J. D.: Chemical characterization of secondary organic aerosol from oxidation of isoprene hydroxyhydroperoxides, Environ. Sci. Technol., 2016, 10.1021/acs.est.6b02511.

St. Clair, J. M., Rivera-Rios, J. C., Crounse, J. D., Knap, H. C., Bates, K. H., Teng, A. P., Jørgensen, S., Kjaergaard, H. G., Keutsch, F. N., and Wennberg, P. O.: Kinetics and products of the reaction of the first-generation isoprene hydroxy hydroperoxide (ISOPOOH) with OH, J. Phys. Chem. A, 2015, 10.1021/acs.jpca.5b06532.

Surratt, J. D., Lewandowski, M., Offenberg, J. H., Jaoui, M., Kleindienst, T. E., Edney, E. O., and Seinfeld, J. H.: Effect of acidity on secondary organic aerosol formation from isoprene, Environ. Sci. Technol., 41, 5363-5369, 2007a, 10.1021/es0704176.

Surratt, J. D., Kroll, J. H., Kleindienst, T. E., Edney, E. O., Claeys, M., Sorooshian, A., Ng, N. L., Offenberg, J. H., Lewandowski, M., Jaoui, M., Flagan, R. C., and Seinfeld, J. H.:

Evidence for organosulfates in secondary organic aerosol, Environ. Sci. Technol., 41, 517-527, 2007b, 10.1021/es062081q.

Thalman, R., in preparation.

Ulbrich, I., Canagaratna, M., Zhang, Q., Worsnop, D., and Jimenez, J.: Interpretation of organic components from Positive Matrix Factorization of aerosol mass spectrometric data, Atmos. Chem. Phys., 9, 2891-2918, 2009, 10.5194/acp-9-2891-2009.

Wong, J. P., Lee, A. K., and Abbatt, J. P.: Impacts of Sulfate Seed Acidity and Water Content on Isoprene Secondary Organic Aerosol Formation, Environ. Sci. Technol., 49, 13215-13221, 2015, 10.1021/acs.est.5b02686.

Worton, D. R., Surratt, J. D., LaFranchi, B. W., Chan, A. W. H., Zhao, Y., Weber, R. J., Park, J.-H., Gilman, J. B., de Gouw, J., Park, C., Schade, G., Beaver, M., Clair, J. M. S., Crounse, J., Wennberg, P., Wolfe, G. M., Harrold, S., Thornton, J. A., Farmer, D. K., Docherty, K. S., Cubison, M. J., Jimenez, J.-L., Frossard, A. A., Russell, L. M., Kristensen, K., Glasius, M., Mao, J., Ren, X., Brune, W., Browne, E. C., Pusede, S. E., Cohen, R. C., Seinfeld, J. H., and Goldstein, A. H.: Observational insights into aerosol formation from isoprene, Environ. Sci. Technol., 47, 11403-11413, 2013, 10.1021/es4011064.

Xu, L., Guo, H., Boyd, C. M., Klein, M., Bougiatioti, A., Cerully, K. M., Hite, J. R., Isaacman-VanWertz, G., Kreisberg, N. M., Knote, C., Olson, K., Koss, A., Goldstein, A. H., Hering, S. V., de Gouw, J., Baumann, K., Lee, S.-H., Nenes, A., Weber, R. J., and Ng, N. L.: Effects of anthropogenic emissions on aerosol formation from isoprene and monoterpenes in the southeastern United States, Proc. Natl. Acad. Sci. USA, 112, 37-42, 2015, 10.1073/pnas.1417609112.

Zhang, Q., Alfarra, M. R., Worsnop, D. R., Allan, J. D., Coe, H., Canagaratna, M. R., and Jimenez, J. L.: Deconvolution and quantification of hydrocarbon-like and oxygenated organic aerosols based on aerosol mass spectrometry, Environ. Sci. Technol., 39, 4938-4952, 2005, 10.1021/es048568l.

Zhang, X., Smith, K. A., Worsnop, D. R., Jimenez, J. L., Jayne, J. T., Kolb, C. E., Morris, J., and Davidovits, P.: Numerical characterization of particle beam collimation: part II integrated aerodynamic-lens–nozzle system, Aerosol Sci. Technol., 38, 619-638, 2004, 10.1080/02786820490479833.

List of Supplementary Figures

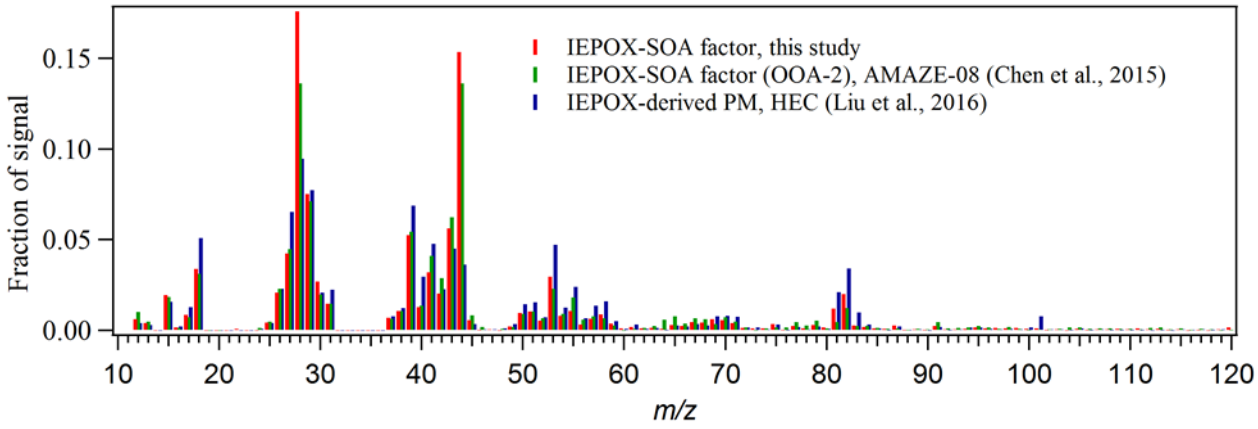

Figure S1. Profile of the IEPOX-SOA factor resolved by PMF analysis of the time series of AMS organic mass spectra collected in the wet season of 2014 (IOP1) at the T3 site (red), and in the wet season of 2008 (green) as part of AMAZE-08 experiment at the T0t site (Chen et al., 2015). Also plotted is the mass spectrum of secondary organic material produced in the Harvard Environmental Chamber from β-IEPOX photooxidation onto acidic ammonium sulfate seed particles under HO_2-dominant conditions and RH < 5% (blue) (Liu et al., 2015). Pearson correlation coefficients *R* between the PMF factor of this study and the other spectra were: *R* = 0.99 for the AMAZE-08 PMF factor, *R* = 0.81 for the chamber spectrum with all ions included, and *R* = 0.95 for the chamber spectrum with *m/z* 44 and 28 excluded.

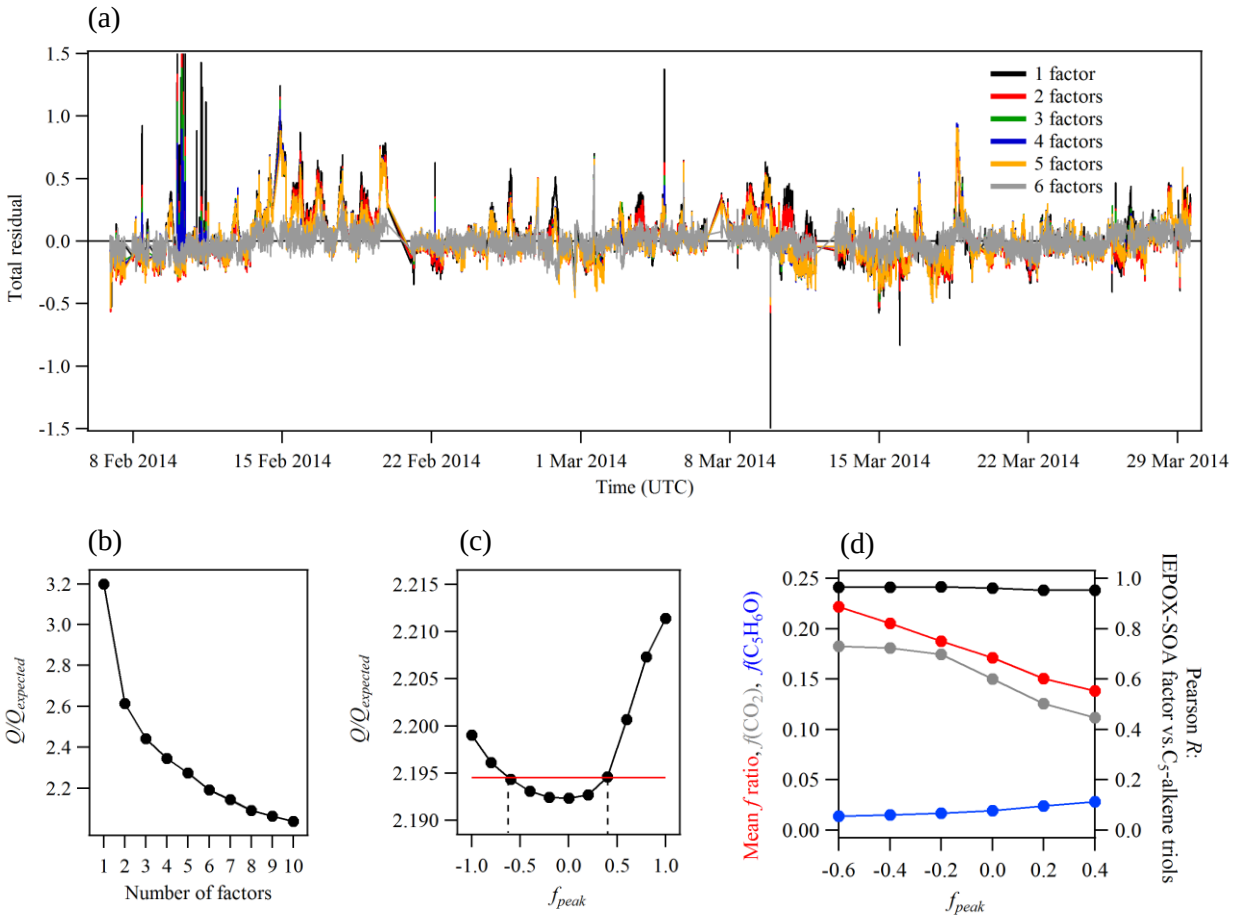

Figure S2. (a) Time series of total ion residuals of PMF solutions from one to six factors, (b) Dependence of the quality-of-fit parameter $Q/Q_{expected}$ on the number of factors for $f_{peak} = 0$, (c) Dependence of the quality-of-fit parameter $Q/Q_{expected}$ on f_{peak} for number of factors = 6. The red line represents $Q/Q_{expected}$ that exceeds in 0.1% the minimum value at $f_{peak} = 0$. This limit determines the range of plausible f_{peak} values as indicated by the dashed black lines, (d) For the six-factor solution, dependence on the f_{peak} parameter of the Pearson correlation coefficient R between the IEPOX-SOA factor loadings and independently measured C_5-alkene triols (on the right vertical axis), the mean f ratio of IEPOX-SOA factor loading to total organic PM mass concentration, and the relative intensities $f(CO_2)$ and $f(C_5H_6O)$of the ions CO_2^+ and $C_5H_6O^+$, respectively (on the left vertical axis).

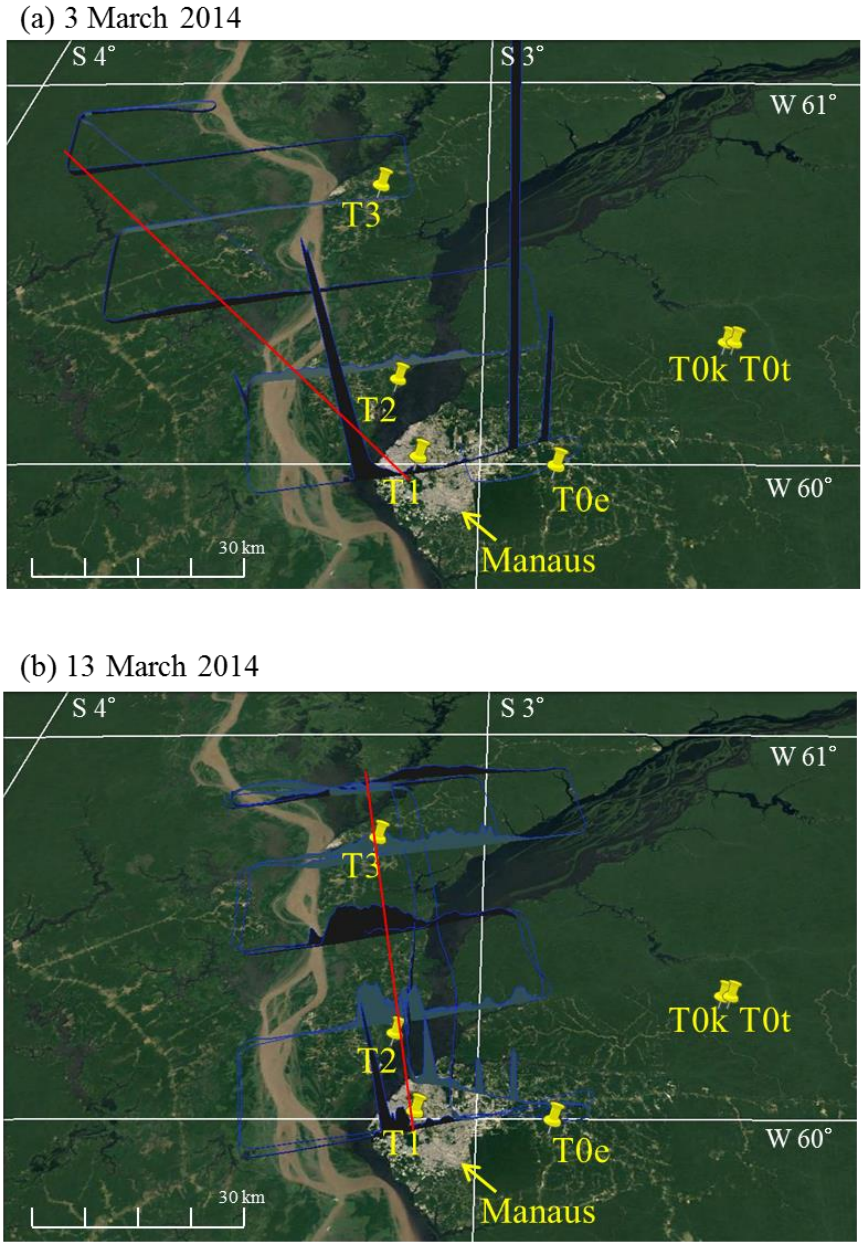

Figure S3. Visualization of the Manaus pollution plume for (a) March 3, 2014, 17:45 – 19:26 UTC, and (b) March 13, 2014, 14:14 – 17:21 UTC. The direction and extent of the plume observed within the boundary layer in the Manaus environs by the G-1 aircraft is represented by plotting NO_y concentrations on a vertical axis (0.13 to 369 ppb on March 3 and 0.10 to 75 ppb on March 13). The red lines guide the eye through the central axis of the plume. An image of land cover is in the horizontal plane. Yellow pins indicate the locations of some of the GoAmazon2014/5 research sites, including T3 (Martin et al., 2016).

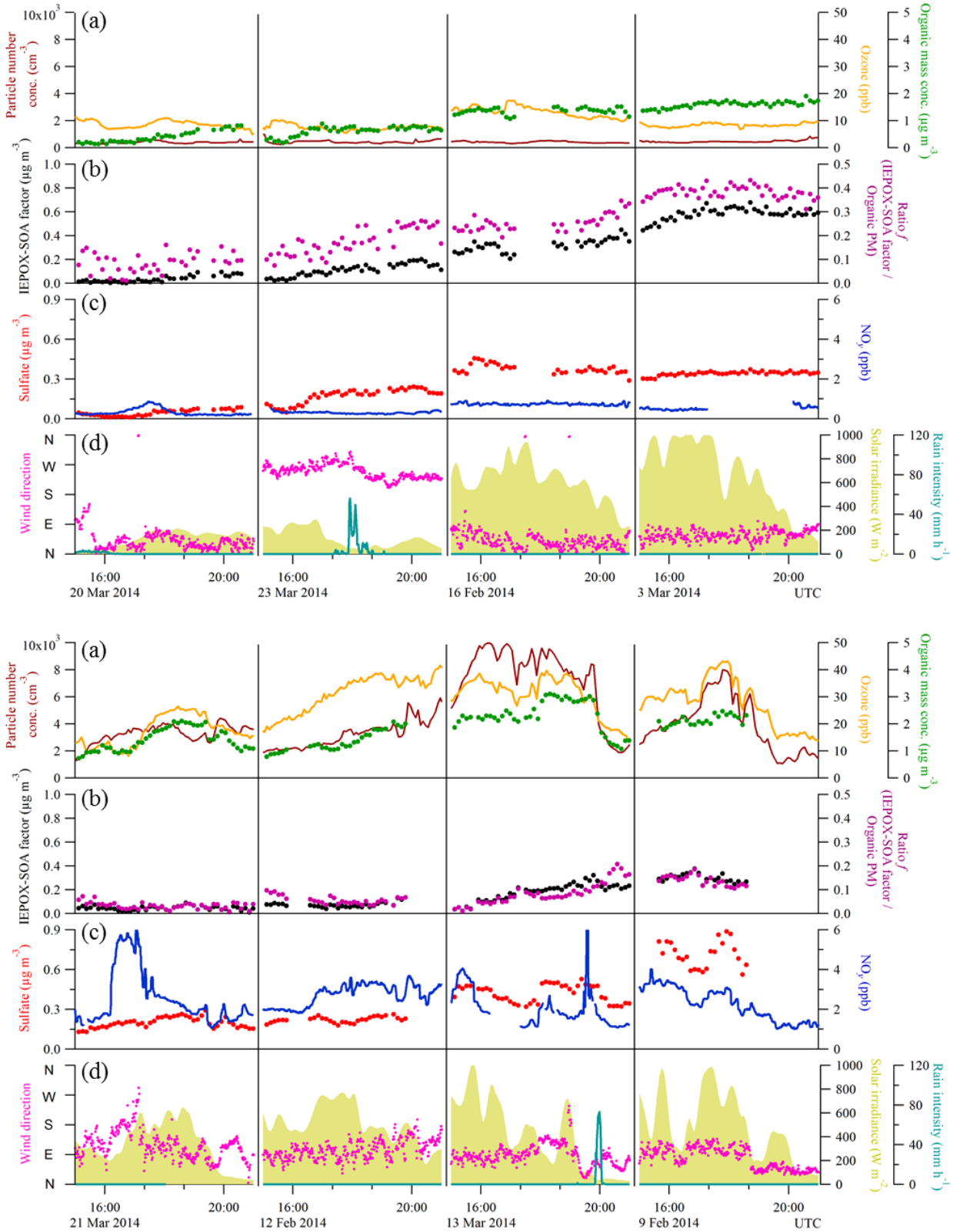

Figure S4. Selected cases of data sets collected during background and polluted conditions (top and bottom panels, respectively) as observed during afternoons at the T3 site.

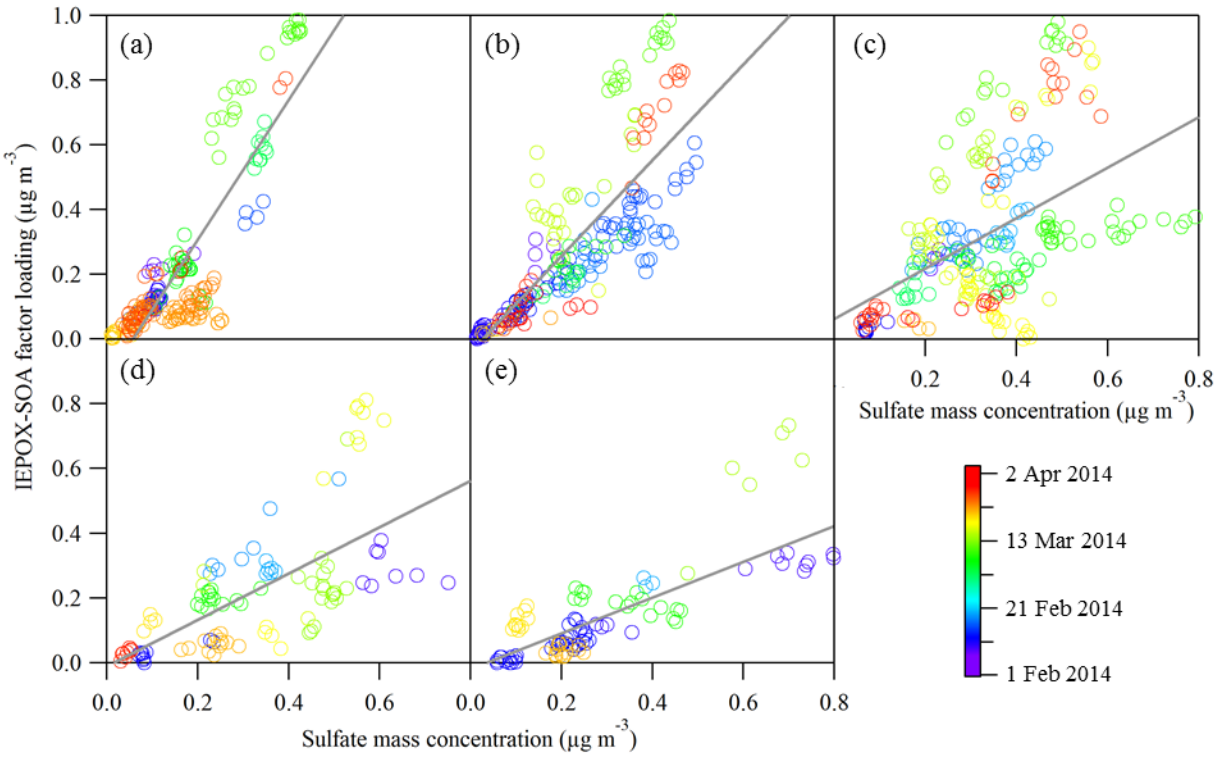

Figure S5. Scatter plots of sulfate mass concentration and IEPOX-SOA factor loading for local afternoon (12:00-16:00 local time; 16:00-20:00 UTC) for five different ranges of NO_y concentrations. Panels a-e correspond to groups labeled 1-5 according to Table 1. Table 1 presents the parameters of the six least-squares linear fits represented by the lines in the figure. Data is colored by date.

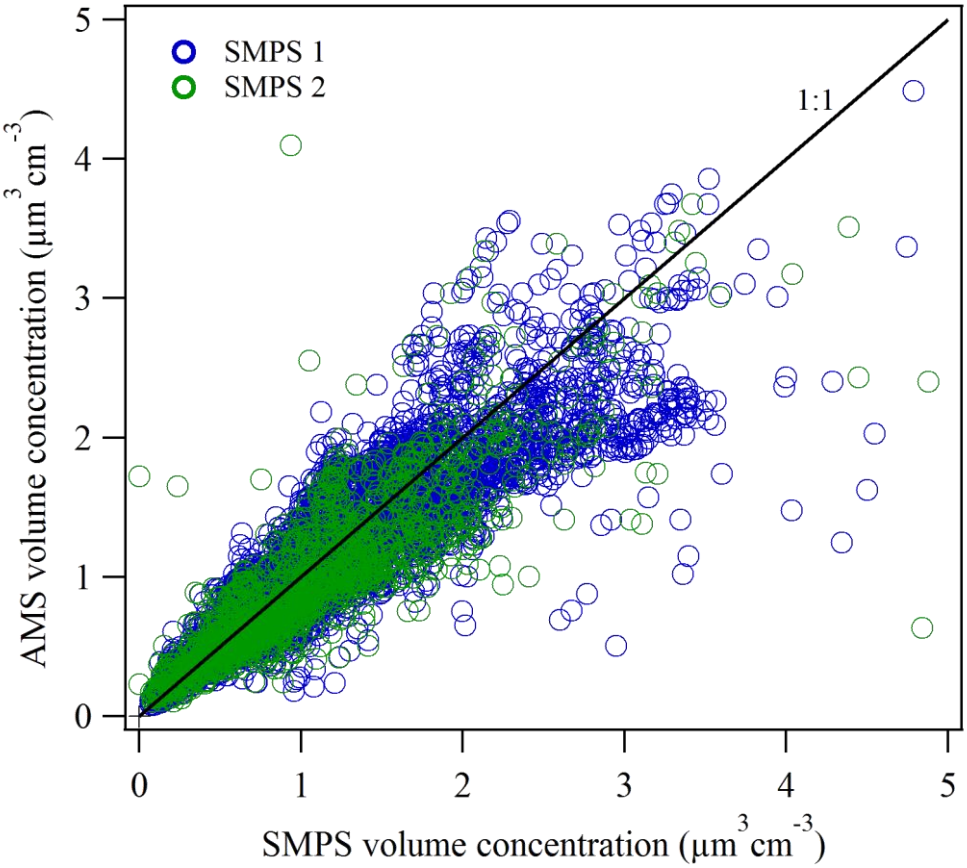

Figure S6. Scatter plot of AMS PM volume concentrations and SMPS PM volume concentrations. SMPS1 measured particles having mobility diameters of 10 to 461 nm from February 7 to March 28, 2014. SMPS2 measured particles having mobility diameters of 10 to 510 nm from February 24 to March 30. Material densities used in the calculation of AMS volume from AMS mass were based on a mixing rule for the five AMS-measured species. The material density of the organic component was calculated following the method of Kuwata et al. (2011) based on O:C and H:C values, which in turn were calculated following the method of Canagaratna et al. (2015).

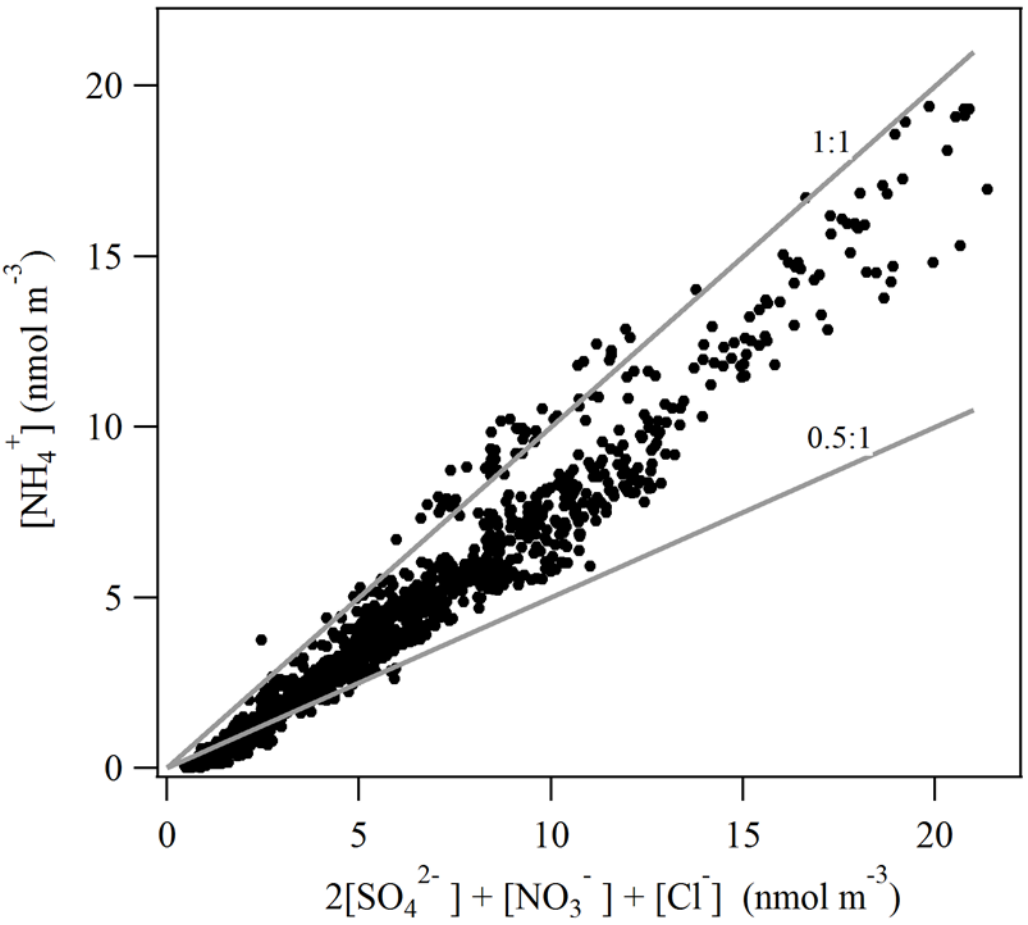

Figure S7. Ion balance for AMS measured species. A scatter plot is shown of mass concentrations of cations on the ordinate and of anions on the abscissa. Solid gray lines indicate relationships of 1:1 and 0.5:1.

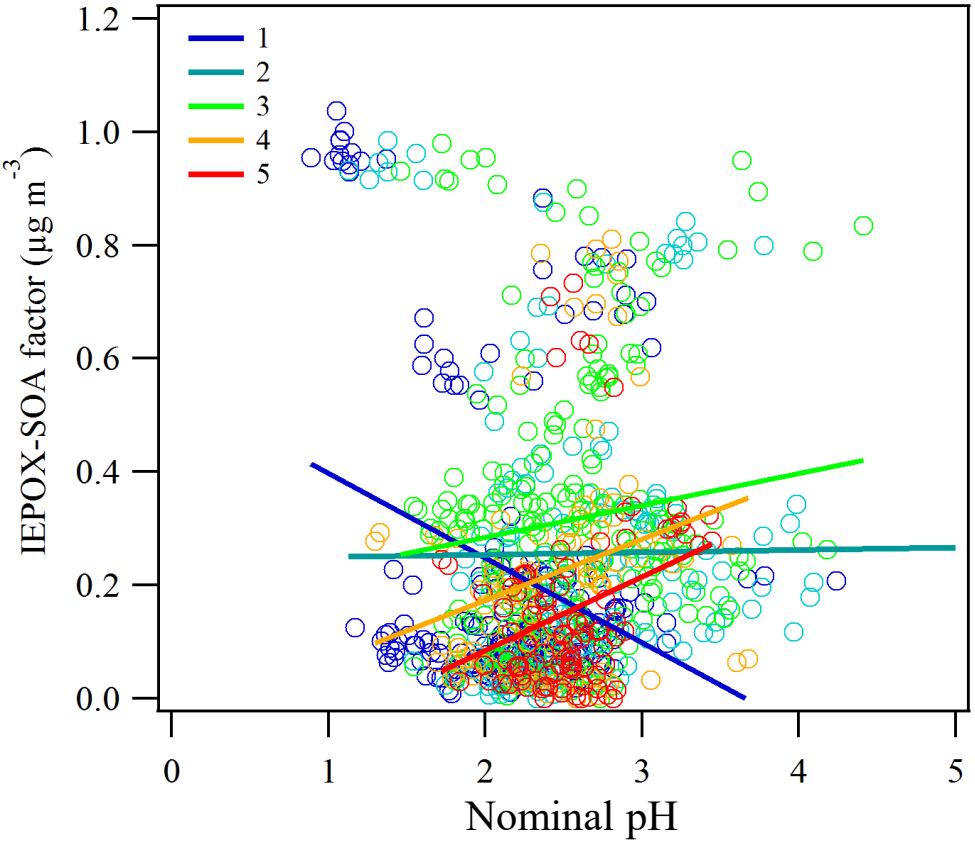

Figure S8. Scatter plot of estimated pH and IEPOX-SOA factor loading for local afternoon (12:00-16:00 local time; 16:00-20:00 UTC). The data sets were collected into five subsets, colored and labeled 1 to 5, based on NO_y concentration (analogous to analysis shown in Figure 6a).

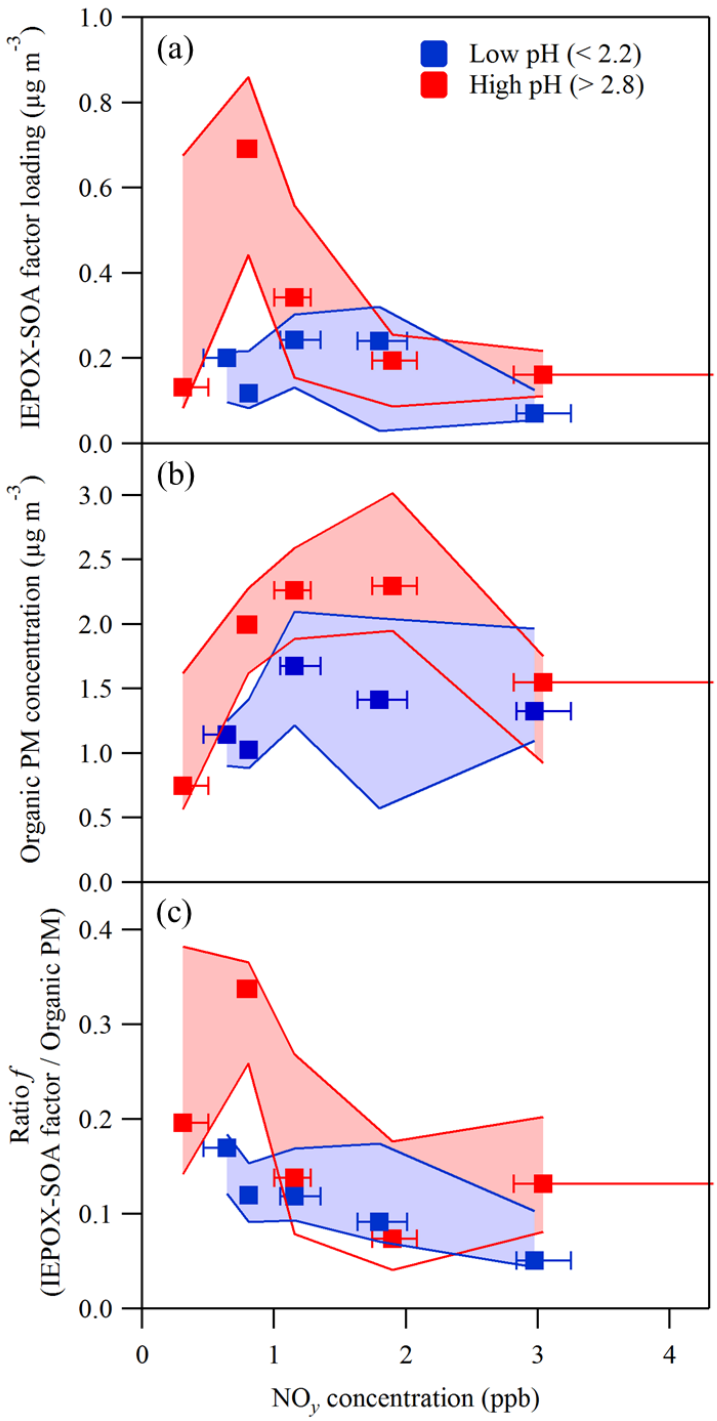

Figure S9. Dependence on NO_y concentration of (a) IEPOX-SOA factor loading, (b) organic mass concentration, and (c) the ratio *f* of the IEPOX-SOA factor loading to the organic PM concentration. Data are segregated by low (< 2.2) and high (> 2.8) pH and grouped into five levels of NO_y concentration (Figure 7). Squares represent medians of each group. Interquartile ranges are represented by whiskers along the abscissa and shading along the ordinate. The plotted data sets were recorded during local afternoon (12:00-16:00 local time; 16:00-20:00 UTC).